Available online at www.sciencedirect.com
ScienceDirect
Journal of Molecular Catalysis A: Chemical 269 (2007) 169–178
JOURNAL OF MOLECULAR CATALYSIS A: CHEMICAL
www.elsevier.com/locate/molcata

Density functional theory study of CO adsorption on the (1 0 0), (0 0 1) and (0 1 0) surfaces of Fe_3C

Xiao-Yuan Liao [a], Dong-Bo Cao [a], Sheng-Guang Wang [a], Zhong-Yun Ma [a], Yong-Wang Li [a], Jianguo Wang [a], Haijun Jiao [a,b,*]

[a] *State Key Laboratory of Coal Conversion, Institute of Coal Chemistry, Chinese Academy of Sciences, Taiyuan, Shanxi 030001, PR China*
[b] *Leibniz-Institut für Katalyse e.V. an der Universität Rostock, Albert-Einstein-Strasse 29a, 18059 Rostock, Germany*

Received 11 September 2006; received in revised form 9 January 2007; accepted 10 January 2007
Available online 14 January 2007

Abstract

Density functional theory (DFT) calculations have been carried out on the adsorption of CO on the (1 0 0), (0 0 1) and (0 1 0) surfaces of Fe_3C. Both (1 0 0) and (0 0 1) have surface iron and carbon atoms, while (0 1 0) has only surface iron atoms. At 1/5 ML on (1 0 0), the most stable adsorption configuration has adsorbed CO at a three-fold site (three Fe atoms), followed by adsorbed surface ketenylidene at a four-fold site (three iron atoms and one carbon atom). At 1/6 ML on (0 0 1), the most stable adsorption configuration has adsorbed CO at a four-fold site (four iron atoms). With increased coverage, adsorption at different sites becomes possible and close in energy. On the metallic (0 1 0) surface, both two-fold and three-fold adsorptions are close in energy. The electronic states of the most stable adsorption structures have been analyzed accordingly.

Keywords: Fe_3C; CO; Adsorption; Fischer-Tropsch synthesis; DFT

1. Introduction

Transition metal carbides have attracted considerable attention because of their excellent physical and chemical properties [1–8], e.g. extreme hardness and brittleness, high melting points and electrical as well as thermal conductivities [9]. In addition, transition metal carbides also are widely used in heterogeneous catalysis [10], and they exhibit strong activity and selectivity, and are resistant to poisoning in hydrogenation [11–13], dehydrogenation [14], hydrodesulfurization [15,16], hydrodenitrogenation [17,18] and Fischer-Tropsch synthesis (FTS) [19–24].

Among iron carbides, Fe_3C is one of the most important active phases of iron-based catalysts in FTS. Transmission electron microscopy (TEM), X-ray diffraction (XRD) and Mössbauer spectroscopy studies indicate that Fe_3C is responsible for the high FTS activity [19–28]. In FTS the degree of carburization of iron-based catalysts correlates well with the catalytic activity during the activation steps [29]. The phases of iron carbides in fused catalysts change with increased temperature. At low temperature (115 °C), $Fe_{2.2}C$ and Fe_2C phases are formed simultaneously, and change to pure Fe_2C at 150–185 °C. They are converted to Fe_5C_2 at 200–400 °C, and finally to the stable Fe_3C phase at 450 °C [30,31]. Apart from iron carbides, small amount of α-Fe and Fe_2O_3 exists in iron-based catalysts [32,33]. Therefore, it is very important and necessary to study the Fe_3C surfaces along with the Fe_5C_2 surfaces [34] for understanding the FTS mechanism.

Chiou and Carter [35] studied the electronic properties of Fe_3C bulk on the basis of density functional theory (DFT) calculation, and found that Fe_3C has a metallic character. Häglund et al. [36] also found that the overall characteristics of Fe_3C are similar to those of pure iron or simple iron carbides (such as FeC). Chiou and Carter [35] also studied the carbide depletion mechanism of Fe_3C in steel material and found (0 0 1) to be the most stable surface, (1 0 0) to be the least stable surface and (0 1 0) to be the intermediate surface.

Many theoretical and experimental studies have focused on CO adsorption on transition metal carbide surfaces [37–45]. It shows clearly that electronic structures play a dominant role in the surface bonding of carbides. Studies of CO adsorption

* Corresponding author at: Leibniz-Institut für Katalyse e.V. an der Universität Rostock, Albert-Einstein-Strasse 29a, 18059 Rostock, Germany.
Tel.: +49 381 1281135; fax: +49 381 12815000.
E-mail address: haijun.jiao@catalysis.de (H. Jiao).

1381-1169/$ – see front matter © 2007 Elsevier B.V. All rights reserved.
doi:10.1016/j.molcata.2007.01.015

on carbides show that CO prefers to interact with Fe atoms on carbide surfaces. Chen et al. [46] found that CO desorbs molecularly on the surface at temperatures above 200 K by temperature-programmed desorption experiments. The formation of carbides reduces the degree of the interaction between the metal d band and the $2\pi^*$ orbital of the adsorbed CO [47]. CO adsorbs dissociatively on ZrC(1 1 1) and on oxygen-modified ZrC(1 0 0) at room temperature [37,38]. St. Clair et al. [39] analyzed the interaction of CO on Mo- and C-terminated α-Mo_2C(0 0 0 1) surfaces, and found that CO adsorbs molecularly. Thermal desorption spectroscopy experiments indicated one CO chemisorption state with an apparent first-order activation energy of 93 kJ/mol for desorption at saturated coverage. DFT study on CO adsorption on both Mo- and C-terminated α-Mo(0 0 0 1) shows that the most stable adsorption has CO capping over the carbon vacancy on the C-terminated surface and atop of surface carbon forming ketenylidene (C=C=O) species on the C-terminated surface [48]. DFT calculations on CO adsorption on the (0 0 1), (1 0 0) and (1 1 0) surfaces of Fe_5C_2 show that CO prefers to adsorb on the three-fold iron site of (0 0 1), the two-fold iron site of (1 1 0), and the three-fold iron site of (1 0 0) at low coverage on the basis of the computed adsorption energies [34]. The adsorption of hydrogen [49] and co-adsorption of CO and hydrogen [50] on the (0 0 1), (1 0 0) and (1 1 0) surfaces of Fe_5C_2 have also been studied theoretically.

Since neither experimental nor theoretical studies of the detailed mechanism of FTS on Fe_3C surfaces are reported, we have used the characteristic (1 0 0), (0 0 1) and (0 1 0) surfaces found by Chiou and Carter [35] for studying CO adsorption. To cast light on the mechanism of CO activation on Fe_3C surfaces, the structures, adsorption energies and the density of states (DOS) of the adsorbed CO were analyzed systematically. It is found that several iron carbide phases are formed simultaneously during FTS, CO adsorption on these phases gives the same vibrational bands, and it is therefore very difficult to identify and distinguish the bulk structures of iron carbides from CO or syngas adsorption [32,51]. On this basis, comparison among CO adsorption on Fe, Fe_5C_2 and Fe_3C has been made.

2. Methods and models

DFT calculations within the generalized gradient approximation (GGA) [52] and the Perdew–Wang 91 functional (PW91) [53] were carried out to study CO chemisorption on the Fe_3C surfaces. All calculations were carried out using the Cambridge Sequential Total Energy Package (CASTEP) [54,55]. Ionic cores were described by the ultrasoft pseudopotential [56]. The Kohn-Sham one-electron states were expanded in a plane wave basis set up to 340 eV. A Fermi smearing of 0.1 eV was utilized. Brillouin zone integration was approximated by a sum over special *k*-points chosen using the Monhorst-Pack scheme [57]. The pseudopotential with partial core was used in spin-polarized calculations to include nonlinear core corrections [58]. Spin polarization having a major effect on the adsorption energies for magnetic systems [59–61] was included to correctly account for the magnetic properties of the ferromagnetic Fe_3C. The vacuum between the slabs was set to span a range of 10 Å to minimize the interaction between the slabs. The convergence criteria for the structure optimization and energy calculation were set to: (a) a self-consistent field tolerance of 2.0×10^{-6} eV/atom; (b) an energy tolerance of 2.0×10^{-5} eV/atom; (c) a maximum force tolerance of 5.0×10^{-2} eV/Å; (d) a maximum displacement tolerance of 2.0×10^{-3} Å. As shown in Fig. 1, Fe_3C has an orthorhombic structure with 16 atoms per unit cell, where 8 iron atoms are in "general" positions (Fe_g), 4 iron atoms are in "special" positions (Fe_s), and 4 carbon atoms are in the interstices. Each Fe_g atom is 14-coordinated with 11 Fe–Fe bonds and 3 Fe–C bonds, and each Fe_s atom is also 14-coordinated but with 12 Fe–Fe bonds and 2 Fe–C bonds [62]. The bulk lattice constant and magnetic moment were calculated to test the method and convergence criteria employed. As shown in Table 1, the calculated bulk lattice constant by three methods agrees well. The lattice constant at PW91 ($a = 5.02$ Å, $b = 6.74$ Å, $c = 4.50$ Å) and the magnetic moment ($Fe_g = 1.88\ \mu_B$ for general iron, and $Fe_s = 1.96\ \mu_B$ for special iron) with *k*-points of $4 \times 3 \times 4$ agree with the experiment ($a = 5.09$, $b = 6.74$, $c = 4.52$) [63], and the average moment of iron atom (1.78 μ_B) [64], and this validates the employed PW91 functional nicely for the Fe_3C system.

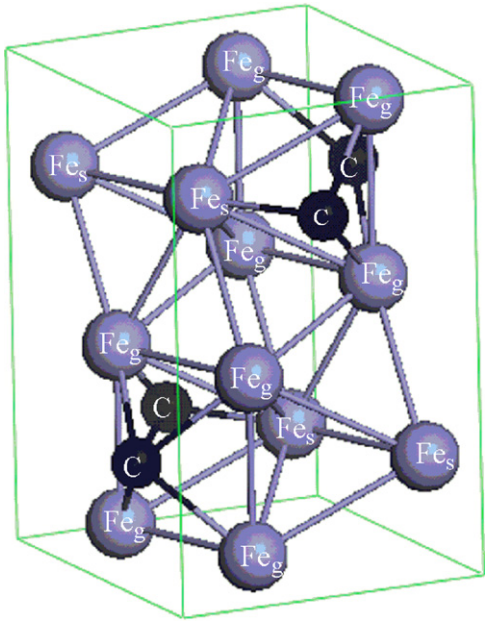

Fig. 1. The unit cell of the cementite Fe_3C.

Table 1
Computed lattice constant (Å) and magnetic moment (μ_B) of Fe_3C

Method	*a*	*b*	*c*	μ_B (Fe_g, Fe_s)[a]
PW91	5.02	6.74	4.50	1.88, 1.96
PBE	5.03	6.73	4.48	1.94, 2.02
RPBE	5.06	6.76	4.51	2.04, 2.06
Expt.[b]	5.09	6.74	4.52	1.78[c]

[a] Magnetic moments per atom, including Fe in general (g) and special (s) positions.
[b] The available experimental values.
[c] Reference [64].

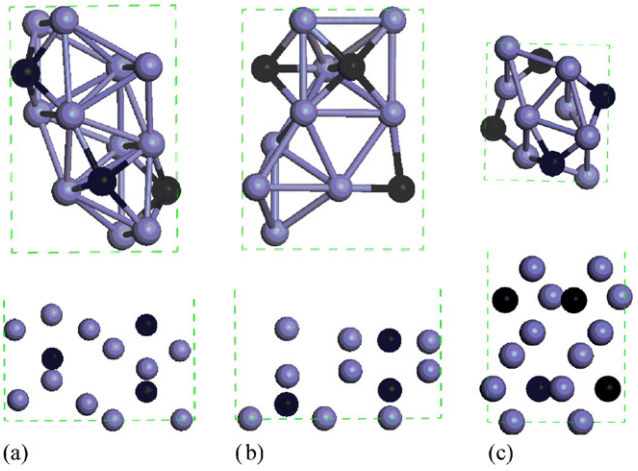

Fig. 2. Top and front views of $Fe_3C(1\,0\,0)$ (a); $Fe_3C(0\,0\,1)$ (b); and $Fe_3C(0\,1\,0)$ (c) in a p(1 × 1) unit cell.

In order to describe the interaction between CO and Fe_3C, we defined the adsorption energy in the following equation: $E_{ads} = [E(n\mathrm{CO/slab}) - (E(\mathrm{slab}) + E(n\mathrm{CO}))]/n$, where the first term is the total energy for the slab with chemisorbed CO on the surface, the second term is the total energy of the bare slab. The third term is the total energy of free CO and n is the number of adsorbed CO molecules. Therefore, the more negative the E_{ads}, the more stable the adsorbed structure. Since revised Perdew–Burke–Ernzerhof (RPBE) can obtain better adsorption energies [48,65–67], single point energy corrections were performed to all of the structures at the RPBE level. In the following sections, we use the RPBE energies for discussion, and the PW91 values are provided for comparison. To understand the bonding nature of the adsorbed CO on Fe_3C, detailed analyses of electronic structure on the basis of density of state were carried out.

As shown in Fig. 2, the $Fe_3C(1\,0\,0)$ model is a slab consisting of seven Fe layers and three C layers (7Fe + 3C). In our calculation, the bottom four Fe layers and one C layer (4Fe + 1C) were fixed in their bulk positions, while the top three Fe layers and two C layers (3Fe + 2C) were allowed to relax. The first layer is composed of Fe atoms, and the second is composed of one exposed C and two exposed Fe atoms. The third layer is composed of two Fe atoms and is also exposed to the surface. A k-point sampling was performed using 3 × 4 × 1 Monkhorst-Pack meshes for the unit cell. In addition, the layer thickness and CO adsorption energies are tested in Table 2. It is found that a slab of seven Fe layers and three C layers (7Fe + 3C) under the relaxation of the top four Fe layers and two C layers (4Fe + 2C) results in energy change of −0.02 and 0.00 eV for **7** and **8**, respectively. A slab of eight Fe layers and four C layers (8Fe + 4C) under relaxation of the top four Fe layers and two C layers (4Fe + 2C) results in energy change of **7** and **8** by 0.04 and 0.00 eV, respectively.

As shown in Fig. 2 and Table 2, $Fe_3C(0\,0\,1)$ model has five Fe layers and three C layers (5Fe + 3C), in which the bottom one Fe layer and two C layers (1Fe + 2C) were fixed in their bulky positions, while the four Fe layers and one C layer on the top (4Fe + 1C) were allowed to relax. The top layer of $Fe_3C(0\,0\,1)$ has one Fe, while the second layer contains two Fe atoms and one C atom. The third, fourth and seventh layers are Fe layers with two, one and three Fe atoms, respectively, while the fifth and sixth layers are composed of only one C atom. A 4 × 3 × 1 k-point sampling within the Brillouin zone was used in the p(1 × 1) unit cell. A model system with six Fe layers and four C layers (6Fe + 4C) under the relaxation of the four Fe layers and one C layer on the top (4Fe + 1C) has a change in adsorption energy of **21** and **26** by −0.06 and −0.03 eV, respectively. A model system with six Fe layers and four C layers (6Fe + 4C) under the relaxation of the four Fe layers and two C layers on the top (4Fe + 2C) has the change in adsorption energy of **21** and **26** by −0.05 and −0.02 eV, respectively.

Table 2
Benchmark of slab thickness and CO adsorption energies

Surface	Total layers[a]	Relaxed layers[b]	E_{ads} (eV)[c]	
(1 0 0)			**7**	**8**
	7Fe + 3C	3Fe + 2C	−1.74 (−2.16)	−1.77 (−2.21)
	7Fe + 3C	4Fe + 2C	−1.76 (−2.13)	−1.77 (−2.16)
	8Fe + 4C	4Fe + 2C	−1.70 (−2.07)	−1.77 (–2.26)
(0 0 1)			**21**	**26**
	5Fe + 3C	4Fe + 1C	−1.62 (−1.95)	−1.79 (−2.19)
	6Fe + 4C	4Fe + 1C	−1.68 (−2.02)	−1.82 (−2.23)
	6Fe + 4C	4Fe + 2C	−1.67 (−2.00)	−1.81 (−2.22)
(0 1 0)			**33**	**35**
	6Fe + 2C	3Fe + 1C	−1.91 (−2.22)	−2.00 (−2.45)
	6Fe + 2C	4Fe + 1C	−1.95 (−2.30)	−1.90 (−2.35)
	8Fe + 3C	3Fe + 1C	−1.94 (−2.22)	−1.91 (−2.22)

[a] Total layer numbers.
[b] Relaxed layer numbers.
[c] PW91 values in parentheses.

As shown in Fig. 2, the $Fe_3C(0\,1\,0)$ slab is composed of six Fe layers and two C layers (6Fe + 2C) with a p(1 × 1) surface unit cell. The bottom two Fe layers and one C layer (3Fe + 1C) were fixed in their bulk positions, while the top three Fe layers and one C layer (3Fe + 1C) were allowed to relax. The top and third layers are only composed of Fe atoms, while the ratio of iron and carbon is 1:1 in the second layer and the C atoms are covered or hidden under the top Fe layer. A k-point sampling of the 4 × 4 × 1 Monkhorst-Pack meshes for the unit cell was used. A slab of seven Fe and two C layers (6Fe + 2C) under the relaxation of the top three Fe layers and one C layer (4Fe + 1C) has a change in adsorption energies for **33** and **35** by −0.04 and 0.10 eV, respectively. A model system with eight Fe layers and three C layers (8Fe + 3C) under the relaxation of the three Fe layers and one C layers on the top (3Fe + 1C) has a change in adsorption energy for **33**, **35** by less than −0.10 eV (Table 2).

3. Results

3.1. CO adsorption on $Fe_3C(1\,0\,0)$

As shown in Fig. 3, there are ten stable structures (**1**–**10**) for the adsorbed CO on $Fe_3C(1\,0\,0)$ at 1/5 ML. The computed adsorption energies, structural parameters, and the occupancy of C 2p orbital are listed in Table 3. In **1**–**4**, CO absorbs on

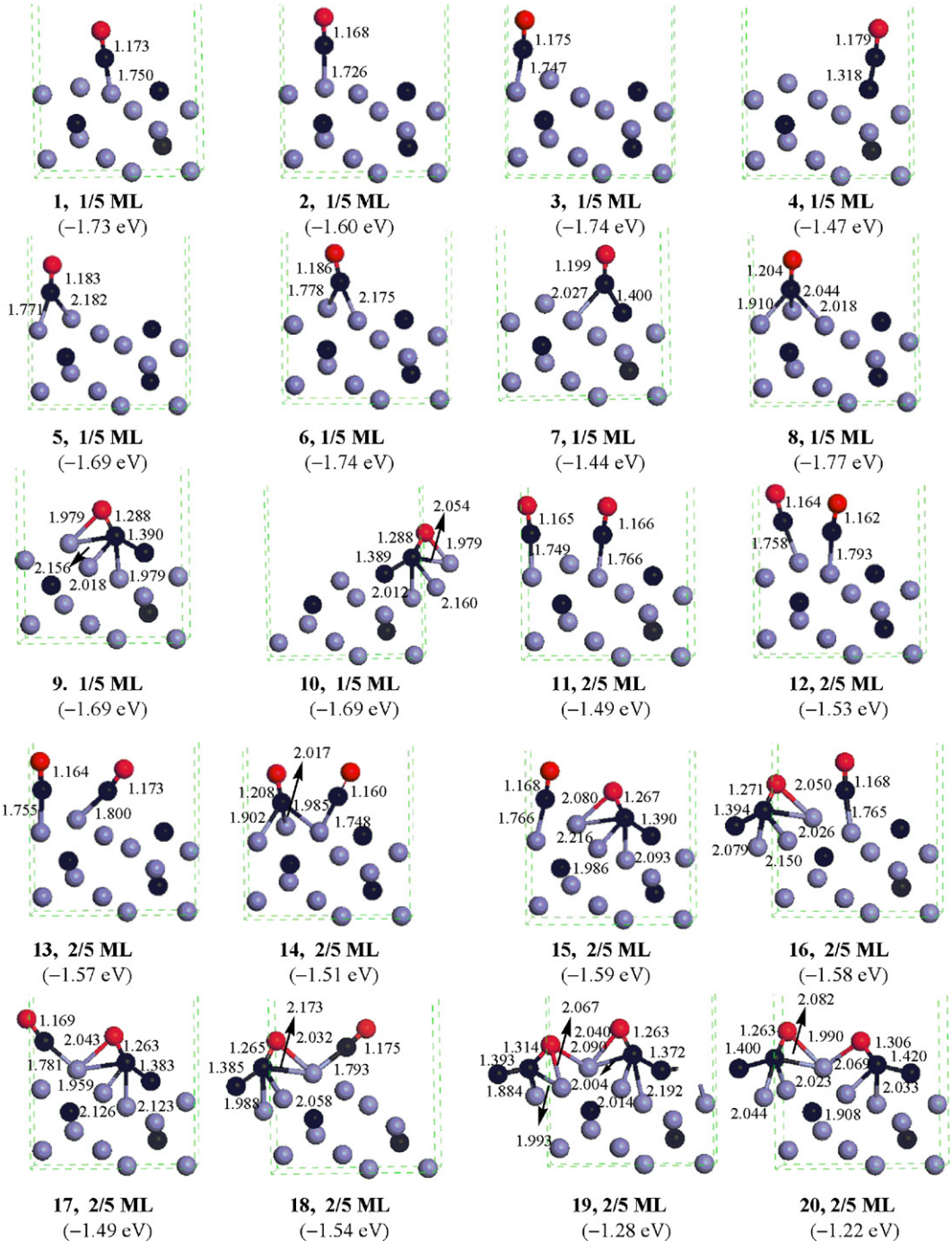

Fig. 3. Adsorption structures of CO on $Fe_3C(1\,0\,0)$.

the top sites. CO binds with one surface Fe atom in **1**–**3**, but with the only surface C atom in **4**. The adsorption energies of **1**–**3** (−1.73, −1.60 and −1.74 eV, respectively) are higher than that of **4** (−1.47 eV). The C–O bond lengths of **1**–**4** are 1.173, 1.168, 1.175 and 1.179 Å, respectively, longer than that of free CO (1.144 Å).

In **5**–**7**, CO absorbs at a two-fold site. In **5** and **6**, CO bonds with two Fe atoms, but with one Fe and one C in **7**. The adsorption energies of **5** and **6** (−1.69, −1.74 eV) are higher than that of **7** (−1.44 eV). The C–O bond lengths in **5**–**7** are 1.183, 1.186 and 1.199 Å, respectively. In **8**, CO absorbs at a three-fold site (three Fe atoms), and the adsorption energy is −1.77 eV. The C–O length of **8** is 1.204 Å. In **9** and **10**, CO absorbs on four-fold sites formed by three Fe atoms and one C atom, and the O atom bonds to one Fe atom, forming surface ketenylidene (CCO). The adsorption energies of **9** and **10** are −1.69 eV. The C–O length of both **9** and **10** is 1.288 Å, being much longer than those of other absorbed structures.

By increasing coverage from 1/5 to 2/5 ML, the adsorption energy decreases, and this is mainly due to the increase in the repulsion interactions between CO molecules. The adsorption energies and structural parameters are also shown in Table 3. In

Table 3
Adsorption energies per CO (eV), bond parameters (d, Å and θ) and C_{2p} occupancy of CO on $Fe_3C(1\,0\,0)$

Species	ML	E_{ads}[a]	d_{C-O}	d_{Fe-C}	d_{C-C}	θ[b]	C_{2p}
1	1/5	−1.73 (−2.11)	1.173	1.750		79	2.57
2	1/5	−1.60 (−1.98)	1.168	1.726		79	2.49
3	1/5	−1.74 (−2.07)	1.175	1.747		87	2.58
4	1/5	−1.47 (−1.72)	1.179		1.318	82	2.73
5	1/5	−1.69 (−2.10)	1.183	1.771, 2.182		76	2.67
6	1/5	−1.74 (−2.16)	1.186	1.778, 2.175		76	2.72
7	1/5	−1.44 (−1.74)	1.199	2.027	1.400	87	2.79
8	1/5	−1.77 (−2.21)	1.204	1.910, 2.044, 2.018		84	2.87
9	1/5	−1.69 (−2.13)	1.288	2.156, 2.018, 1.979	1.390	64	2.99
10	1/5	−1.69 (−2.13)	1.288	2.012, 2.160, 2.054	1.389	54	2.97
11	2/5	−1.49 (−1.84)	1.165	1.749		80	2.51
			1.166	1.766		80	2.50
12	2/5	−1.53 (−1.88)	1.162	1.793		77	2.45
			1.164	1.758		75	2.48
13	2/5	−1.57 (−1.93)	1.164	1.755		51	2.52
			1.173	1.800		85	2.61
14	2/5	−1.51 (−1.91)	1.160	1.748		80	2.46
			1.208	1.902, 2.017, 1.985		80	2.87
15	2/5	−1.59 (−1.98)	1.168	1.766		81	2.58
			1.267	2.216, 1.986, 2.093	1.390	56	2.98
16	2/5	−1.58 (−1.98)	1.168	1.765		69	2.58
			1.271	2.079, 2.150, 2.026	1.394	31	2.99
17	2/5	−1.49 (−1.89)	1.169	1.781		52	2.57
			1.263	1.959, 2.126, 2.123	1.383	57	2.99
18	2/5	−1.54 (−1.94)	1.175	1.793		39	2.64
			1.265	1.988, 2.058, 2.173	1.385	57	2.99
19	2/5	−1.28 (−1.78)	1.263	2.004, 2.014, 2.192	1.372	56	3.01
			1.314	1.884, 1.993, 2.067	1.393	46	2.97
20	2/5	−1.22 (−1.71)	1.263	2.044, 2.023, 2.082	1.400	59	3.00
			1.306	1.908, 2.033	1.420	49	2.92

[a] Values in parentheses are derived from the PW91 functional.
[b] Angle between the CO axis and the y axis.

11–**13**, both CO molecules adsorb on top sites, and their adsorption energies are −1.49, −1.53 and −1.57 eV, respectively. In **14**, one CO occupies a top site and another CO on a three-fold site, and the adsorption energy is −1.51 eV. In **15**–**18**, one CO absorbs on a top and another one on a four-fold site (three Fe atoms and one C atom), and the adsorption energies are −1.59, −1.58, −1.49 and −1.54 eV, respectively. In **19** and **20**, both CO molecules absorb on four-fold sites (three Fe atoms and one C atom), and their adsorption energies are −1.28 and −1.22 eV, respectively. The adsorption energies of **12**–**18** are very close, but stronger than those of **19** and **20**. This indicates the increased repulsive interaction of the four-fold adsorption with increased coverage. Experimentally Guczi [68] found the co-existence of molecularly adsorbed CO on carbide surfaces during FTS.

Further insights into the bonding mechanism of CO on $Fe_3C(1\,0\,0)$ can be obtained by analyzing the DOS of the adsorbed CO molecules. Fig. 4 shows the computed DOS for **1**, **6**, **8** and **10**. The 5σ orbital of free CO is at the Fermi level. For **1**, the 5σ orbital of adsorbed CO shifts downward to −6.27 eV

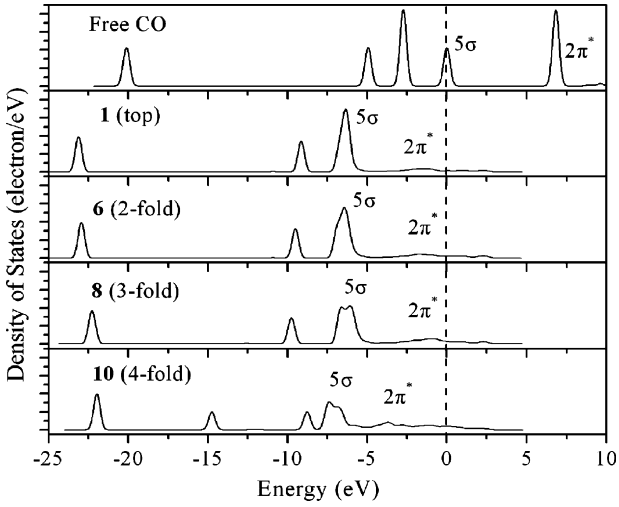

Fig. 4. DOS of free and adsorbed CO on $Fe_3C(1\,0\,0)$ at 1/5 ML.

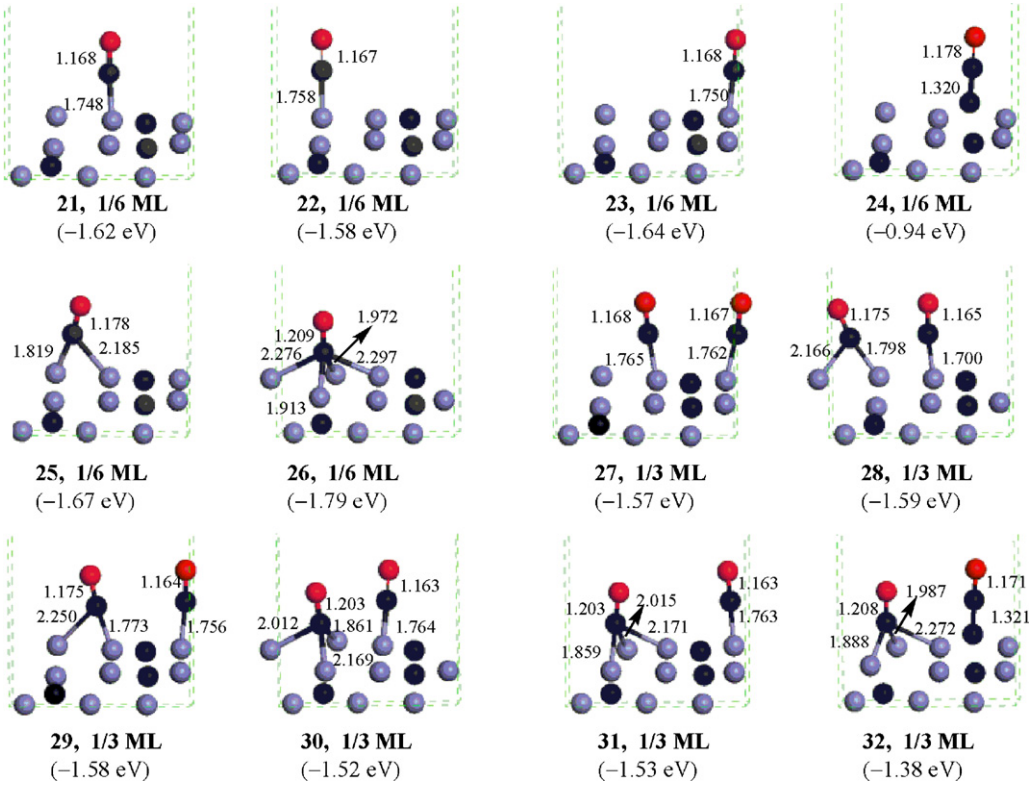

Fig. 5. Adsorption structures of CO on $Fe_3C(0\,0\,1)$.

and the $2\pi^*$ orbital shifts downward to −1.51 eV. The shifts of 5σ and $2\pi^*$ are primarily the results of the 5σ donation and $2\pi^*$ back-donation [47]. The partial charge transfer leads to the broadening of the $2\pi^*$ band with an edge below the Fermi level, and the significant elongation of the C–O bond is due to the anti-bonding nature of the $2\pi^*$ orbital. In addition, the integral of the DOS curve is calculated, and the peak next to $2\pi^*$ represents more than four electrons (the largest occupancy of the degenerated 1π is four electrons) [69]. So it is obvious that the 5σ band shifts downward and overlaps with the 1π band. The 1π bond is thought to be localized in the total DOS and does not take part in the binding progress. For adsorption on a two-fold site in **6**, the $2\pi^*$ orbital of adsorbed CO of shifts downward to −1.75 eV, and the 5σ orbital shifts downward to −6.39 eV. For adsorption on a three-fold site in **8**, the 5σ and $2\pi^*$ orbitals of **8** shift downward to −6.21 and −1.11 eV, respectively. For adsorption on a four-fold site in **10**, and the peak at −15 eV is due to the formation of C–C bond, the peak at about −7.30 eV is due to the formation of Fe–O bond. The $2\pi^*$ orbital of adsorbed CO in **10** shifts downward to −3.72 eV, quite below the Fermi level, indicating a very large charge transfer to CO. The stronger the electron transfer, the stronger the C–O activation [70]. This result is in line with the C–O bond length in **10** of 1.288 Å. Mulliken population analysis shows that the electron population of the C 2p orbital of free CO is 1.90 e, while the electron population of the C 2p orbital of CO in **10** is 2.97 e, higher than the electronic population of C 2p in **1**, **6** and **8** (2.57, 2.72 and 2.87 e). In turn, the C–O bond of **10** is longer than those of other forms. It has been observed that the C–O bond is largely weakened due to the strong d-$2\pi^*$ back-donation when CO is adsorbed on the four-fold site on Fe(0 0 1) [71].

3.2. CO adsorption on $Fe_3C(0\,0\,1)$

There are six adsorbed structures of CO on the surface at 1/6 ML. The calculated adsorption energies and bond parameters for adsorbed CO are listed in Fig. 5 and Table 4. In **21**–**24**, CO adsorbs on top sites. In **21**–**23**, CO binds with one Fe atom, while with surface C atom in **24**. The adsorption energies of **21**–**23** (−1.62, −1.58 and −1.64 eV, respectively) are higher than that

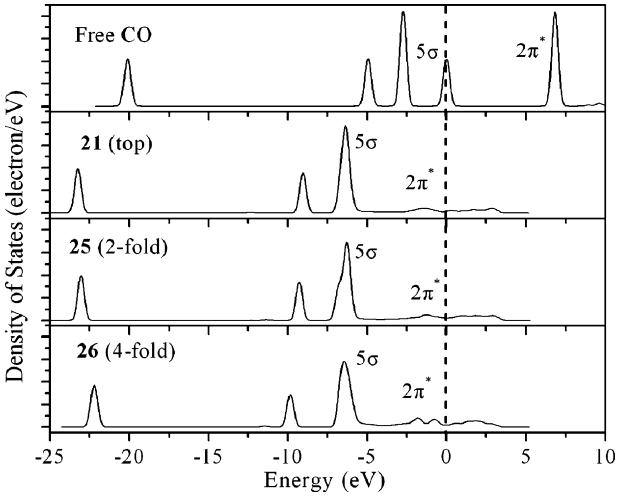

Fig. 6. DOS of free and adsorbed CO on $Fe_3C(0\,0\,1)$.

Table 4
Adsorption energies per CO (eV), bond parameters (d, Å and θ) and C_{2p} occupancy of CO on $Fe_3C(0\,0\,1)$

Species	ML	E_{ads}[a]	d_{C-O}	d_{Fe-C}	d_{C-C}	θ[b]	C_{2p}
21	1/6	−1.62 (−1.95)	1.168	1.748		88	2.53
22	1/6	−1.58 (−1.94)	1.167	1.758		80	2.53
23	1/6	−1.64 (−1.96)	1.168	1.750		89	2.54
24	1/6	−0.94 (−1.15)	1.178		1.320	78	2.71
25	1/6	−1.67 (−2.00)	1.178	1.819, 2.185		66	2.67
26	1/6	−1.79 (−2.19)	1.209	2.276, 1.913, 1.972, 2.297		78	2.89
27	1/3	−1.57 (−1.94)	1.167	1.762		82	2.51
			1.168	1.765		83	2.53
28	1/3	−1.59 (−1.94)	1.165	1.700		76	2.53
			1.175	2.166, 1.798		68	2.65
29	1/3	−1.58 (−1.96)	1.164	1.756		89	2.48
			1.175	2.250, 1.773		74	2.61
30	1/3	−1.52 (−1.91)	1.163	1.764		75	2.47
			1.203	2.012, 2.169, 1.861		78	2.85
31	1/3	−1.53 (−1.91)	1.163	1.763		80	2.48
			1.203	1.859, 2.015, 2.171		77	2.85
32	1/3	−1.38 (−1.68)	1.171		1.321	82	2.64
			1.208	1.888, 1.987, 2.272		82	2.87

[a] Values in parentheses are derived from the PW91 functional.
[b] Angle between the CO axis and y axis.

of **24** (−0.94 eV). The C–O bond lengths of **21**–**24** are 1.168, 1.167, 1.168 and 1.178 Å, respectively. In **25**, CO is absorbed on a two-fold site and the adsorption energy is −1.67 eV. The C–O bond length of **25** is 1.178 Å. In **26**, CO adsorbs on a four-fold site, and the adsorption energy (−1.79 eV) is the highest and the C–O band length of **26** (1.209 Å) is the longest in all adsorbed forms at 1/6 ML.

At the 1/3 ML coverage, both CO molecules adsorb on top sites in **27**, and the adsorption energy is −1.57 eV. In **28** and **29**, one CO adsorbs on a top site and another one on a two-fold site, and the adsorption energy is −1.59 and −1.58 eV, respectively. In **30** and **31**, one CO absorbs on a top site and another one on a three-fold site, while in **32** one CO adsorbs on a three-fold site and another one on the top site of the surface carbon. The

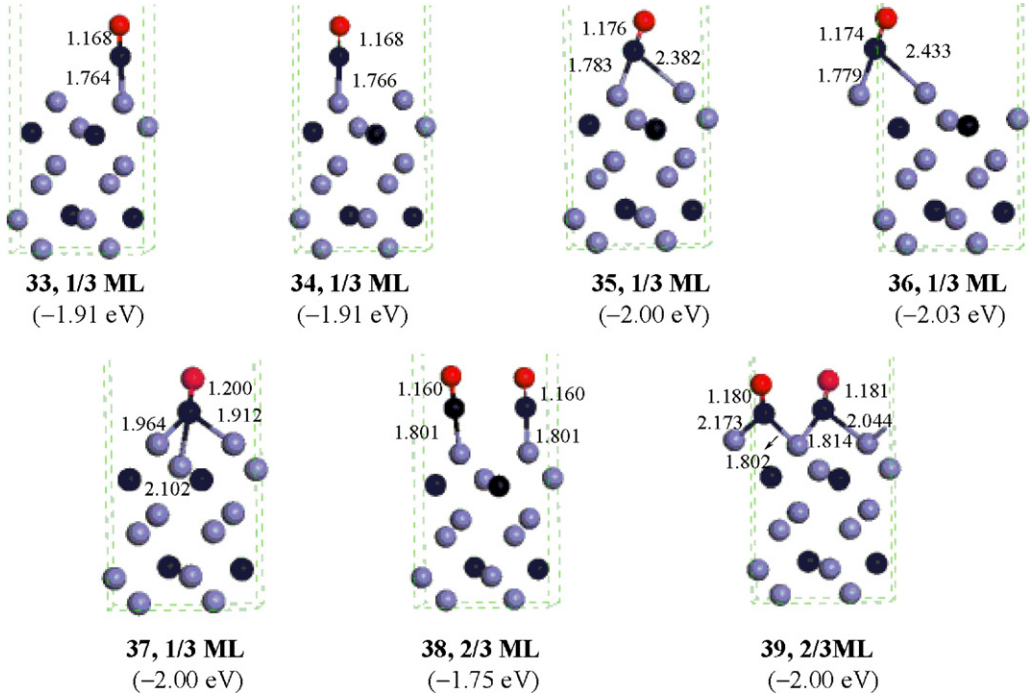

Fig. 7. Adsorption structures of CO on $Fe_3C(0\,1\,0)$.

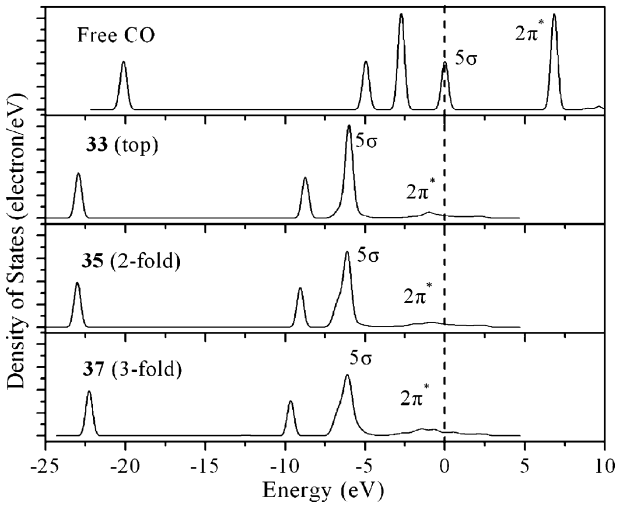

Fig. 8. DOS of free and adsorbed CO $Fe_3C(0\,1\,0)$ at 1/3 ML.

adsorption energies of **30**–**32** are −1.52, −1.53 and −1.38 eV, respectively.

The DOS of adsorbed CO of **21**, **25** and **26** is shown in Fig. 6. All the bands of the adsorbed CO shift downward. The 5σ band of the adsorbed CO shifts below −6.0 eV and overlaps with the 1π band. The $2\pi^*$ orbital is broadened by the partial charge transfer and shifts below the Fermi level. The 5σ and $2\pi^*$ bands of **21** shift downward to −6.32 and −1.37 eV respectively. In **25** and **26**, 5σ band shifts downward to −6.30 and −6.48 eV, and $2\pi^*$ band shifts downward to −1.30 and −1.75 eV, respectively. Similarly, the 5σ donation is important for CO adsorption on TiC [72]. For comparison, the site of $2\pi^*$ band in **26** is lower than that in other forms at this coverage. This result consists with the fact that the C–O bond of adsorbed CO of **26** is the longest (1.209 Å) at this coverage. As given in Table 4, the electronic population of C 2p orbital in **26** (2.89 e) is higher than those in **21**–**25**. As a result, the C–O bond length in **26** is longer than those in **21**–**25**.

3.3. CO adsorption on $Fe_3C(0\,1\,0)$

Since the carbon atoms are buried under iron atoms on $Fe_3C(0\,1\,0)$, CO can only adsorbs on surface Fe. There are five stable structures (**33**–**37**) on this surface at 1/3 ML. The computed bond parameters are listed in Fig. 7 and in Table 5. At 1/3 ML, there are two top adsorbed forms (**33**, **34**), two two-fold forms (**35**, **36**) and one three-fold forms (**37**). In **33**–**37**, the CO adsorption energies of **33** and **34** (−1.91 eV) are the lowest, while that of **36** (−2.03 eV) is the highest at this coverage. The C–O bond lengths in **33** and **34** (1.168 Å) are the shortest among **33**–**37**, while that in **37** (1.200 Å) is the longest. When the coverage of CO increases to 2/3 ML, there are two stable structures (**38** and **39**). In **38**, CO adsorbs on top sites, and the adsorption energy is −1.75 eV. In **39**, CO adsorbs on a two-fold site, and the adsorption energy is −2.00 eV.

The DOS of CO in **33**, **35** and **37** is shown in Fig. 8. In **33**, the 5σ and $2\pi^*$ orbitals shift downward to −6.01 and −1.00 eV, respectively. In **35**, 5σ orbital shifts downward to −6.09 eV, and $2\pi^*$ orbital shifts downward to −1.16 eV. In **37**, 5σ and $2\pi^*$ bands shift downward to −6.01 and −1.51 eV, respectively. The site of $2\pi^*$ orbital in **37** is the lowest among **33**, **35** and **37**. As shown in Table 5, the electronic population of C 2p orbital in **37** (2.86 e) is the largest among **33**–**37**. Accordingly, the C–O bond length in **37** is the longest among **33**–**37**. The large charge transfer to CO leads to the weakened C–O bonds.

4. Summary and discussion

CO adsorption on the $Fe_3C(1\,0\,0)$, $(0\,0\,1)$ and $(0\,1\,0)$ surfaces at different coverages has been investigated on the basis of density of functional theory calculations. For CO adsorption on $Fe_3C(1\,0\,0)$, $(0\,0\,1)$, and $(0\,1\,0)$, there are various adsorption structures, and new species ketenylidene (CCO). Thus, we compare the adsorption energy and C–O bond activation on the three surfaces.

When CO (1/5 ML) is only bonded with surface Fe atom, the highest adsorption energy are −1.77 eV (**8**) on $(1\,0\,0)$ at three-fold, −1.79 eV (**26**) on $(0\,0\,1)$ at four-fold, and −2.03 eV (**36**) on $(0\,1\,0)$ at two-fold, respectively. The C–O bond lengths in **8**, **26** and **36** are 1.204, 1.209 and 1.174 Å, respectively. Thus, the CO adsorption energy on $(0\,1\,0)$ is the highest among three surfaces. These differences are mainly due to the surface structure and composition, e.g. $(1\,0\,0)$ and $(0\,0\,1)$ have surface carbon atoms, while $(0\,1\,0)$ surface has only surface iron atoms.

Table 5
Adsorption energies per molecule (eV) and structures (d, Å and θ) and C_{2p} occupancy of CO on the $Fe_3C(0\,1\,0)$ surface

Species	ML	E_{ads} [a]	d_{C-O}	d_{Fe-C}	θ [b]	C_{2p}
33	1/3	−1.91 (−2.22)	1.168	1.764	89	2.55
34	1/3	−1.91 (−2.21)	1.168	1.766	87	2.54
35	1/3	−2.00 (−2.45)	1.176	1.783, 2.382	88	2.63
36	1/3	−2.03 (−2.46)	1.174	1.779, 2.433	87	2.58
37	1/3	−2.00 (−2.49)	1.200	1.964, 2.102, 1.912	67	2.86
38	2/3	−1.75 (−2.12)	1.160	1.801	68	2.44
			1.160	1.801	75	2.50
39	2/3	−2.00 (−2.43)	1.180	2.173, 1.802	61	2.76
			1.181	1.814, 2.044	61	2.76

[a] Values in parentheses are derived from the PW91 functional.
[b] Angle between the CO axis and y axis.

It is interesting to note the four-fold (**9** and **10**) CO adsorption with the formation of surface ketenylidene (CCO) species on (1 0 0), which may be the precursor of CO dissociation. Indeed, Joseph et al. confirmed the existence of the ketenylidene functionality by ^{13}C NMR spectroscopy, and proposed the migration of a carbon monoxide onto the exposed carbide atom to form a ketenylidene [73]. The existence of C=C=O has been verified by a recent in situ IR spectra study of CO adsorbed on fresh β-Mo_2C [74]. In addition, similar surface species of N=C=O on the γ-Mo_2N(1 0 0) surface was proposed both experimentally [75] and theoretically [76]. That the surface C–C bonds are important for exchange of carbon and the C–C coupling on the surfaces in FTS has been verified by Stockwell et al. with ^{13}C traces [77], and they found that surface carbon atoms of carbide catalysts are incorporated into the FTS products. Furthermore, Jiang et al. found that carbonaceous species forms on the Fe/Mn surface when some surface Fe atoms are converted to iron carbide, and the carbonaceous species shields the detection of the Fe sites by probe adsorption [78]. All these indicate that the participation of surface C sites plays an essential role in many reactions on metal carbide surfaces. At higher CO coverage (2/5 ML), the most stable configurations have both four-fold and atop adsorbed CO molecules. In addition, **9** and **10** are very close to **8** in adsorption energy, indicating the possible co-existence or equilibrium.

For CO adsorbed at surface carbon atoms at atop sites, the adsorption energy is −1.47 eV (**4**) on Fe_3C(1 0 0) and −0.94 eV (**24**) on Fe_3C(0 0 1) surfaces. The corresponding C–O bond lengths are 1.179 and 1.178 Å, respectively. Compared to CO adsorption on surface Fe, CO adsorption at atop carbon atoms is not favored. This is in agreement with CO adsorption on the Mo- and C-terminated α-Mo_2C(0 0 0 1) surfaces [48], e.g. the highest adsorption energy is −2.23 eV on the Mo-terminated surface, and only −1.74 eV on the C-terminated surface.

Although Fe_3C(1 0 0) and Fe_3C(0 0 1) have surface carbon, they differ in adsorption structures and energies. At low coverage, the most stable adsorption has three-fold CO on Fe_3C(1 0 0), and four-fold CO on Fe_3C(0 0 1). In addition, Fe_3C(1 0 0) also has four-fold adsorbed CCO species, while Fe_3C(0 0 1) does not. At higher coverage, the most stable adsorption on Fe_3C(0 0 1) has atop, two-fold, and three-fold adsorbed CO molecules.

In contrast, the Fe_3C(0 1 0) surface has only iron atoms. At 1/3 ML, all adsorption structures with adsorbed CO at top, two-fold, and three-fold are close in energy and therefore, they can co-exist or can be in equilibrium. At 2/3 ML coverage, CO adsorption on two-fold sites is more favored.

It is to be noted that the computed adsorption energy for one CO molecule has the order of Fe_3C(0 1 0) > Fe_3C(1 0 0) > Fe_3C(0 0 1), while the surface stability has the order of Fe_3C(0 0 1) > Fe_3C(0 1 0) > Fe_3C(1 0 0) [35]. For Fe_3C(0 0 1) and Fe_3C(1 0 0) with both surface iron and carbon atoms, the less stable Fe_3C(1 0 0) has larger adsorption energy, while the more stable Fe_3C(0 0 1) has smaller adsorption energy. This is in line with the relationship between stability and reactivity.

It is also interesting to compare the most stable CO adsorption forms on different Fe and Fe_5C_2 surfaces with those on Fe_3C (Table 6). It shows clearly that at the RPBE level the CO adsorption energies on Fe(1 0 0) and Fe(1 1 0) are overestimated by 0.38 and 0.34 eV, respectively, as compared with the available experimental data. These differences can be used to scale the computed results. It shows also that both RPBE and experiments have the same energetic order of Fe(1 1 0) over Fe(1 0 0) by 0.09 and 0.13 eV, respectively. On the basis of this agreement, it is concluded that Fe(1 1 1) has the strongest CO adsorption energy on clean Fe surfaces. In addition, the scaled CO adsorption energy on Fe(1 1 1) should be around −1.7 to −1.8 eV; unfortunately no experimental data are available yet.

Table 6
Comparison of the largest adsorption energies for CO adsorbed on Fe, Fe_5C_2 and Fe_3C at low coverage

Surface	Method	Site	E_{ads} (eV)	q_{CO} (e)[a]	Ref.
Fe					
(1 0 0)	RPBE	Four-fold	−1.49		[79]
	PBE	Four-fold	(−2.08)		
	PW91	Four-fold	[−2.03]		[80]
	Expt.		−1.11		[79,81]
(1 1 0)	RPBE	Top	−1.58		[82,83]
	PBE	Top	(−1.88)		
	PW91	Top	[−1.95]		
	Expt.		−1.24		[82,84]
(1 1 1)	RPBE	Shallow–hollow	−2.08	−0.46	[85]
	PBE		(−2.45)		[69]
Fe_5C_2					
(1 0 0)	PBE	Three-fold	(−2.21)	−0.52	[34]
(0 0 1)	PBE	Three-fold	(−2.10)	−0.45	
(1 1 0)	PBE	Three-fold	(−2.34)	−0.54	
Fe_3C					
(1 0 0)	RPBE	Three-fold	−1.77	−0.57	This work
	PW91		[−2.21]		
(0 0 1)	RPBE	Four-fold	−1.79	−0.57	
	PW91		[−2.19]		
(0 1 0)	RPBE	Two-fold	−2.03	−0.32	
	PW91		[−2.46]		

[a] This value is obtained from the Mulliken charge of the adsorbed CO probe.

On the basis of the fact that both PBE and PW91 have similar CO adsorption energies on the clean Fe surface, it is to be expected that this relationship can also be extrapolated to the Fe_5C_2 and Fe_3C surface. On this basis, CO adsorption on Fe_5C_2 and Fe_3C should have similar adsorption properties [32,51]. It shows clearly that both Fe_5C_2(1 1 0) and Fe_3C(0 1 0) surfaces with only surface iron atoms have the strongest CO adsorption energies as compared with the surfaces with both surface iron and carbon atoms. It is to be noted that CO adsorption on Fe(1 1 1) has nearly the same adsorption as on Fe_3C(0 1 0), while those on Fe_3C(1 0 0)/Fe_3C(0 0 1) and Fe_5C_2(1 0 0) and Fe_5C_2(0 0 1) are stronger than on Fe(1 0 0) and Fe(1 1 0). Table 6 shows the Mulliken charges of the adsorbed CO. It shows that pure metallic surfaces with stronger CO adsorption affinity have lower degree of charge transfer of the adsorbed CO than those with both surface iron and carbon atoms. In addition, surfaces with both surface iron and carbon atoms have a close degree of charge transfer of the adsorbed CO.

Acknowledgments

This work was supported by Chinese Academy of Sciences and the National Natural Science Foundation of China (Nos. 20473111 and 20590361); and the National Outstanding Young Scientists Foundation of China (No. 20625620).

References

[1] S.P. Dodd, G.A. Saunders, M. Cankurtaran, B. James, M. Acet, Phys. Stat. Sol. (a) 198 (2003) 272.
[2] Y.F. Zhang, J.Q. Li, L.X. Zhou, Surf. Sci. 488 (2001) 256.
[3] I. Kojima, E. Miyazaki, J. Catal. 89 (1984) 168.
[4] L. Bugyi, A. Oszkó, F. Solymosi, Surf. Sci. 519 (2002) 139.
[5] S.V. Meschel, O.J. Kleppa, J. Alloys Compd. 257 (1997) 227.
[6] A.J. Scott, R. Brydson, M. MacKenzie, A.J. Craven, Phys. Rev. B 63 (2001) 245105.
[7] P. Liu, J. Rodriguez, J. Chem. Phys. 120 (2004) 5414.
[8] R.S. DaBell, R.G. Meyer, M.D. Morse, J. Chem. Phys. 114 (2001) 2938.
[9] J.A. Nelson, M.J. Wagner, Chem. Mater. 14 (2002) 4460.
[10] S.T. Oyama, The Chemistry of Transition Metal Carbides and Nitrides, Blackie, Glasgow, UK, 1996.
[11] M. Saito, R.B. Anderson, J. Catal. 63 (1980) 438.
[12] G.S. Ranhotra, A.T. Bell, J.A. Reimer, J. Catal. 108 (1987) 40.
[13] J.S. Lee, M.H. Yeom, D.-S. Lee, J. Mol. Catal. A 62 (1990) L45.
[14] F. Solymosi, R. Németh, Catal. Lett. 62 (1999) 197.
[15] S.T. Oyama, C.C. Yu, S. Ramanathan, J. Catal. 184 (1999) 535.
[16] J.A. Rodriguez, J. Dvorak, T. Jirsak, Surf. Sci. 457 (2000) L413.
[17] T.E. Lucy, T.P. St. Clair, S.T. Oyama, J. Mater. Res. 13 (1998) 2321.
[18] V. Schwartz, V.T. Da Silva, S.T. Oyama, J. Mol. Catal. A 163 (2000) 251.
[19] V. Carles, P. Alphonse, P. Tailhades, A. Rousset, Thermochim. Acta 334 (1999) 107.
[20] J.W. Niemantsverdriet, A.M. van der Kraan, W.L. van Dijk, H.S. van der Baan, J. Phys. Chem. 84 (1980) 3363.
[21] G.L. Caer, J.M. Dubois, J.P. Senateur, J. Solid State Chem. 19 (1976) 19.
[22] H. Bemas, I.A. Campbell, R. Fruchart, J. Phys. Chem. Solids 28 (1967) 17.
[23] R.B. Anderson, The Fisher-Tropsch Synthesis, Academic Press, New York, 1984.
[24] Y. Jin, A.K. Datye, J. Catal. 196 (2000) 8.
[25] D. Mahajan, P. Gutlich, J. Ensling, K. Pandya, U. Stumm, P. Vijayaraghavan, Energy Fuels 17 (2003) 1210.
[26] A.A. Mirzaei, R. Habipour, M. Faizi, E. Kashi, Appl. Catal. A 301 (2006) 272.
[27] P.H. Emmett (Ed.), Crystallite Phase and Their Relationship to Fischer-Tropsch Catalysis, Reinhold, New York, 1956, p. 407.
[28] T. Herranz, S. Rojas, F.J. Pérez-Alonso, M. Ojeda, P. Terreros, J.L.G. Fierro, J. Catal. 243 (2006) 199.
[29] M.D. Shroff, D.S. Kalakkad, K.E. Coulter, S.D. Kohler, M.S. Harrington, N.B. Jackson, A.G. Sault, A.K. Datye, J. Catal. 156 (1995) 185.
[30] J.A. Amelse, J.B. Butt, L.H. Schwartz, J. Phys. Chem. 82 (1978) 558.
[31] A. Königer, C. Hammerl, M. Zeitler, B. Rauschenbach, Phys. Rev. B 55 (1997) 8143.
[32] G. Bian, A. Oonuki, N. Koizumi, H. Nomoto, M. Yamada, J. Mol. Catal. A 186 (2002) 203.
[33] C.H. Bartholomew, M.W. Stoker, L. Mansker, A.K. Datye, Stud. Surf. Sci. Catal. 126 (1999) 265.
[34] D.-B. Cao, F.-Q. Zhang, Y.-W. Li, H. Jiao, J. Phys. Chem. B 108 (2004) 9094.
[35] W.C. Chiou Jr., E.A. Carter, Surf. Sci. 530 (2003) 87.
[36] J. Häglund, G. Grimavall, T. Jarlborg, Phys. Rev. B 44 (1996) 2914.
[37] H.H. Hwu, J.G. Chen, Chem. Rev. 105 (2005) 185.
[38] T. Nakane, T. Noda, K. Ozawa, K. Edamoto, Surf. Sci. 435 (1999) 180.
[39] T.P. St. Clair, S.T. Oyama, D.F. Cox, Surf. Sci. 468 (2000) 62.
[40] S.A. Jansen, R. Hoffmann, Surf. Sci. 197 (1988) 474.
[41] C. Oshima, M. Aono, T. Tanaka, S. Kawai, S. Zaima, Y. Shibata, Surf. Sci. 102 (1981) 312.
[42] M.L. Colaianni, J.G. Chen, W.H. Weinberg, J.T. Yates Jr., J. Am. Chem. Soc. 114 (1992) 3735.
[43] S.V. Didziulis, P. Frantz, L. Fernandez-Torres, R.L. Gnenard, O. Elbjeirami, S.S. Perry, J. Phys. Chem. B 105 (2001) 5196.
[44] J. Brillo, R. Sur, H. Kuhlenbeck, H.-J. Freund, Surf. Sci. 397 (1998) 137.
[45] J. Wang, M. Castonguay, J. Deng, P.H. McBreen, Surf. Sci. 374 (1997) 197.
[46] J.G. Chen, B.D. DeVries, B. Fruhberger, C.M. Kim, Z.M. Liu, J. Vac. Sci. Technol. A 13 (1995) 1600.
[47] S.-S. Sung, R. Hoffmann, J. Am. Chem. Soc. 107 (1985) 578.
[48] J. Ren, C.-F. Huo, J. Wang, Y.-W. Li, H. Jiao, Surf. Sci. 596 (2005) 212.
[49] D.-B. Cao, F.-Q. Zhang, Y.-W. Li, J.G. Wang, H. Jiao, J. Phys. Chem. B 109 (2005) 833.
[50] D.-B. Cao, F.-Q. Zhang, Y.-W. Li, J.G. Wang, H. Jiao, J. Phys. Chem. B 109 (2005) 10922.
[51] S.A. Eliason, C.H. Bartholomew, Appl. Catal. A 186 (1999) 229.
[52] J.A. White, D.M. Bird, Phys. Rev. B 50 (1994) 4954.
[53] J.P. Perdew, J.A. Chevary, S.H. Vosko, K.A. Jackson, M.R. Pederson, D.J. Singh, C. Fiolhais, Phys. Rev. B 46 (1992) 6671.
[54] M.C. Payne, D.C. Allan, T.A. Arias, J.D. Joannopoulos, Rev. Mod. Phys. 64 (1992) 1045.
[55] V. Milman, B. Winkler, J.A. White, C.J. Pickard, M.C. Payne, E.V. Akhmataskaya, R.H. Nobes, Int. J. Quantum Chem. 77 (2000) 895.
[56] D. Vanderbilt, Phys. Rev. B 41 (1990) 7892.
[57] H.J. Monkhorst, J.D. Pack, Phys. Rev. B 13 (1976) 5188.
[58] S.G. Louie, S. Froyen, M.L. Cohen, Phys. Rev. B 26 (1982) 1738.
[59] H. Cheng, D.B. Reiser, S.W. Dean Jr., K. Baumert, J. Phys. Chem. B 105 (2001) 12547.
[60] Q. Ge, M. Neurock, H.A. Wright, N. Srinivasan, J. Phys. Chem. B 106 (2002) 2826.
[61] Q. Ge, S.J. Jenkins, D.A. King, Chem. Phys. Lett. 327 (2000) 125.
[62] I.R. Shein, N.I. Medvedeva, A.L. Ivanovskii, Phys. B 371 (2006) 126.
[63] E.J. Fasiska, G.A. Jeffrey, Acta Crystallogr. 19 (1965) 463.
[64] I.N. Shabanova, V.A. Trapeznikov, JETP Lett. 18 (1973) 339.
[65] B. Hammer, L.B. Hansen, J.K. Nørskov, Phys. Rev. B 59 (1999) 7413.
[66] Y. Zhang, W. Yang, Phys. Rev. Lett. 80 (1998) 890.
[67] C.-F. Huo, Y.-W. Li, J. Wang, H. Jiao, J. Phys. Chem. B 109 (2005) 14160.
[68] L. Guczi, Catal. Rev. Sci. Eng. 23 (1981) 329.
[69] Y.-H. Chen, D.-B. Cao, J. Yang, Y.-W. Li, J. Wang, H. Jiao, Chem. Phys. Lett. 400 (2004) 35.
[70] S.-G. Wang, D.-B. Cao, Y.-W. Li, J. Wang, H. Jiao, J. Phys. Chem. B 109 (2005) 18956.
[71] S.K. Nayak, M. Nooijen, S.L. Bernasek, P. Blaha, J. Phys. Chem. B 105 (2001) 164.
[72] S.V. Didziulis, K.D. Butcher, S.S. Perry, Inorg. Chem. 42 (2003) 7766.
[73] W.K. Joseph, M.H. Elizabeth, F.S. Duward, J. Am. Chem. Soc. 105 (1983) 7307.
[74] W. Wu, Z. Wu, C. Liang, X. Chen, P. Ying, C. Li, J. Phys. Chem. B 107 (2003) 7088.
[75] S. Yang, Y. Li, C. Ji, C. Li, Q. Xin, J. Catal. 174 (1998) 34.
[76] G. Frapper, M. Pélissier, J. Hafner, Appl. Catal. A 134 (1996) 339.
[77] D.M. Stockwell, D. Bianchi, C.O. Bennett, J. Catal. 113 (1988) 13.
[78] M. Jiang, N. Koizumi, M. Yamada, J. Phys. Chem. B 104 (2000) 7636.
[79] D.E. Jiang, E.A. Carter, J. Phys. Chem. B 110 (2006) 22213.
[80] D.C. Sorescu, D.L. Thompson, M.M. Hurley, C.F. Chbalowski, Phys. Rev. B 66 (2002) 035416.
[81] (a) D.W. Moon, D.J. Dwyer, S.L. Bernasek, Surf. Sci. 163 (1985) 215; (b) S.D. Cameron, F.J. Dwyer, Langmuir 4 (1988) 282.
[82] D.E. Jiang, E.A. Carter, Surf. Sci. 570 (2004) 167.
[83] A. Stibor, G. Kresse, A. Eichler, J. Hafner, Surf. Sci. 507 (2002) 99.
[84] G. Wedler, R. Ruhmann, Appl. Surf. Sci. 14 (1983) 137.
[85] C.-F. Huo, J. Ren, Y.-W. Li, J. Wang, H. Jiao, J. Phys. Chem. B, unpublished result.